Design of an Artificial Muscle Actuated Finger towards Biomimetic Prosthetic Hands

Vishalini Bundhoo and Edward J. Park, *Member, IEEE*

Abstract — **This paper focuses on the design and modeling of a prosthetic finger for children. Conventional prosthetic hands are simple grippers that only restore the very basic grasping capabilities of the human hand. Novel design methodologies are required in order to address the issue of low functionality of prosthetic hands while still meeting their mass and size requirements. We propose a biomimetic approach to prosthetic hand design. The musculosketal characteristics of the human hand are studied in order to extract elements that are essential in the design of a biomechanically accurate hand. This paper presents a 4 DOF finger design that closely mimics the size and kinematics of the human finger. Our design proposes to use SMA-driven tendon wires that are directly attached to the finger structure, in a manner similar to the natural tendons and muscles. A kinematic analysis of the proposed finger, which defines the relationship between the motion of its joints and the corresponding SMA artificial muscle contraction ranges, is presented. The results of a torque analysis, carried out to evaluate SMA wire diameter and actuation forces required, is also presented.**

Index Terms — **Prosthetic hand, biomimetic design, artificial muscle, shape memory alloys (SMA)**

I. Introduction

THE hand is one of the most important parts of the human body. It is the organ that allows for a number of tasks: adaptation, exploration, prehension, perception and manipulation[1]. The hand's functional uniqueness has been recognized and discussed extensively in the literature. With over 20 degrees of freedom (DOF), it also been recognized as being a worthwhile model for emulation as a robotic interface with the environment. Over the last decades, a number of robotic hands have been developed that employ the prehension, manipulation and sensory capabilities of the human hand. Some of the most relevant developments include the Belgrade USC Hand, an anthropomorphic end-effector with four identical 3 DOF fingers and a 2 DOF thumb [2]; the three-fingered Stanford/JPL hand, which possessed 3 DOF in each finger mechanism [3]; the UTAH/MIT hand which had three 4 DOF fingers and a 4 DOF thumb, with each finger driven by eight tendons [4].

The design methodologies and knowledge developed for these robotic hands have been applied to prosthetic hands to improve their performance. However, highly dexterous artificial hands commonly require the use of bulky actuators and complex transmission mechanisms, elements that do not fit the strict mass and size restrictions of prosthetic hands. In fact, prosthetic hands have challenging and conflicting designs specifications, which often cannot be achieved using existing artificial hand technologies. As such, commercially available prosthetic hands, such as the Vasi Hand or the OttoBock Sensor hand, remain simple grippers with only 1 or 2 DOFs. Typically, these hands offer minimum functional restoration of the lost hand with a simple open-close motion. Furthermore, the fingers are rigid with no flexibility. Adaptive grasping, the ability of the fingers to conform to the shape of an object held within the hand, is not possible resulting in low grip stability with respect to external disturbances [5]. Hand prostheses are also relatively heavy compared to the natural hand owing to the use of bulky actuators and complex transmission systems. Moreover, the limited number of DOFs of conventional prostheses causes unnatural, robot-like motion of the fingers, which renders prostheses cosmetically unappealing to the user [5]. Surveys indicate that 30% to 50% of upper extremity amputees do not make use of their prostheses owing to the above deterring factors [6].

Our research ideology is to overcome the shortcomings of conventional prostheses by utilizing a biomimetic (i.e., life-like) approach to prosthetic hand design. This involves mimicking the human hand's architectural and functional characteristics in order to produce an anthropomorphic hand that presents similar grasping, manipulation and tactile abilities as the human hand. The emergence of active materials, such as Electroactive Polymers (EAPs) or Shape Memory Alloys (SMAs), that are operationally similar to the human muscle, have encouraged the development of such biomimetic hands. These materials have allowed the potential development of artificial muscle actuators that mimic the hand muscles. These lightweight, direct-driven actuators provide ways to increase the functionality of artificial hands without adding to bulkiness or mechanical complexity.

This paper focuses on the design of a biomimetic finger, which is to be actuated using SMA artificial muscles. Our ultimate goal is developing a prosthetic hand for children. In fact, in addition to the above addressed drawbacks of conventional hands, children's prostheses are scaled-down models of the adult version. Studies indicate that the discomfort and poor appearance of such prostheses result in children

The authors are with the Department of Mechanical Engineering, University of Victoria, PO BOX 3055 STN CSC, Victoria, BC V8W 3P6 (corresponding author: V. Bundhoo, phone: 250-721-6292, fax: 250-721-6051, email:vish@me.uvic.ca).

0-7803-9177-2/05/$20.00/©2005 IEEE

rejecting them in favor of a more cosmetic but stationary hand, or to abandon the use of the prosthesis altogether [7]. Hence, the biomimetic finger is designed to replicate as closely as possible the size of a child's finger. The natural hand muscles, tendons and their architecture are studied in order to design a biomechanically accurate finger. The proposed finger is a 4 DOF tendon-driven mechanism, which mimics the kinematics and functionality of the human finger. Kinematic and static force analyses are carried out to determine the SMA artificial muscle actuator properties.

II. Physiology of the Human Hand

The human hand consists of five digits, four fingers and a thumb. The fingers constitute of three intercalated bony segments: the proximal, intermediate and distal phalanges. The thumb, on the other hand, lacks the intermediate phalanx and is made up of only the proximal and distal phalanges. The proximal phalange is the first phalange and is connected to the metacarpal bones, which are the bones that form the palm of the hand. The distal phalange is located at the finger end. The joints of the finger are the metacarpophanlangeal (MCP) joint, the proximal interphalangeal (PIP) joint and the distal interphalangeal (DIP) joint. The bones and joints of the hand are illustrated in Fig. 1.

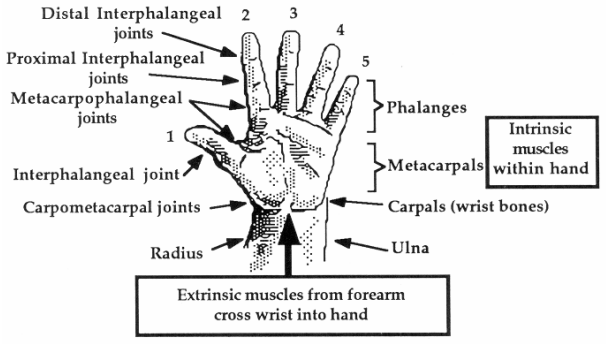

Fig. 1. Bones and joints of the hand [2]

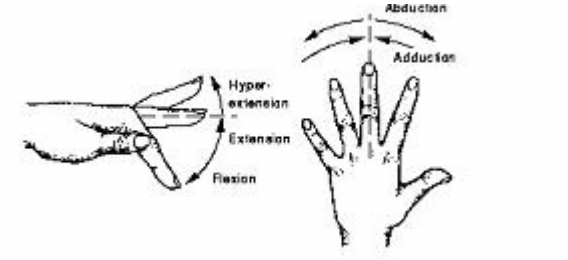

Fig. 2. Finger movements[1]

Fig. 2 illustrates the possible movements of the MCP joint, which is a 2 DOF universal joint that provides abduction/adduction and extension/flexion motions. The PIP and DIP joints are 1 DOF revolute joints, providing extension/flexion. The DIP joint is, however, a passive DOF that follows the movements of the PIP joint through tendons connecting the two joints.

The index finger is found to have the greatest range of extension/flexion amongst the five fingers: 90^o at the MCP joint, $100^o \sim 110^o$ at the PIP joint and 80^o at the DIP joint. In addition, adduction and abduction angles of 20^o have been measured at the MCP joint of the fingers [8].

III. Tendon Network in the Human Finger

Since we are interested in mimicking the actuation mechanism of the human finger, its physiology needs to be studied. As shown in Fig. 3, the index finger is actuated by three intrinsic muscles (2 IO, 1 LU) and four extrinsic muscles through long tendons (EDC, EIP, FDS, FDP). Heavy-lifting extrinsic muscles are located in the forearm, whereas the intrinsic muscles are located in the hand. The intrinsic muscles are less powerful muscles responsible for adduction/abduction and finer dexterous motions of the fingers. The muscles are connected to finger bones through tendons, which are parallel-fibered connective tissues. The tendon network provides indirect actuation of the fingers, acting as a transmission mechanism. The collagen-based tendons are elastic and help return the finger to the original position after flexion or extension. The tendon positions are maintained relative to the phalanges during finger motion by bands of fibers referred to as sheaths, which enable the smooth action of the finger [9].

Flexor tendons are those that close the fingers. The main flexor tendons are the FDS (flexor digitorum superficialis) and FDP (flexor digitorum profundus). The FDS attaches to the base of the middle phalanx while the FDP attaches to the distal phalanx. The FDS flexes the PIP joint, whereas the FDP flexes both the PIP and DIP joints. The MCP flexion is achieved with the help of the extensor hood, shown in Fig 3. The intrinsic LU (lumbrical) and IO (interosseous) muscles are connected to the hood. As these muscles contract, the hood structure hugs the proximal phalanx and initiates flexion of the MCP.

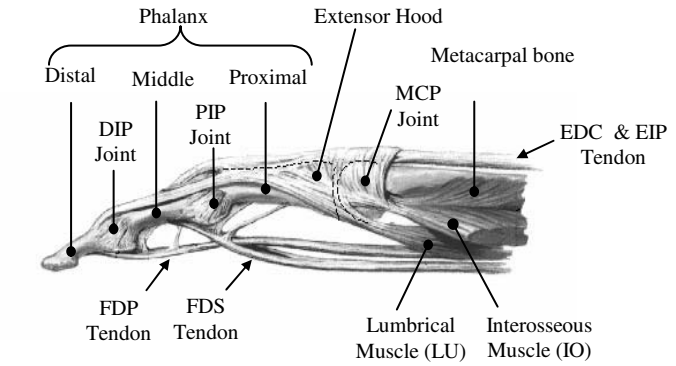

Fig. 1. Muscles and tendons of the index finger

[1] http://www.cse.unsw.edu.au/~waleed/thesis/node17.html

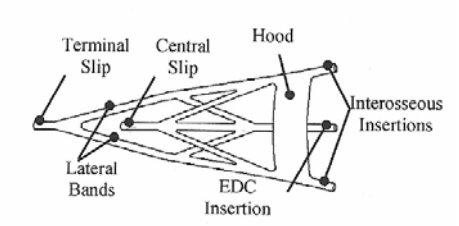

Fig. 4. Extensor mechanism within human finger [10]

Extensor tendons are responsible for the opening of the fingers. As shown in Fig. 4, these tendons form a web-like structure that rides the dorsal side of the finger and connects all the tendons to the three finger bones [10]. The main extensor is the EDC (extensor digitorum). This tendon merges with extensor hood after which, it separates into three bands: the central slip and the two lateral bands. Active contraction of the EDC pulls the hood proximally over the MCP joint and extends that joint. Tension in the EDC also produces extension at both the PIP and DIP joints.

The intrinsic IO and LU muscles do not only assist the extrinsic flexors in flexing the MCP joint, but also assist the extrinsic extensors in extending the MCP, PIP and DIP joints. In fact, neither the EDC nor the IO and LU muscles can produce joint extension independently. Both extrinsic and intrinsic muscles need to act together [8]. Furthermore, the IO muscles work in opposition and control the adduction and abduction motions of the finger.

The lateral bands have multiple functions: they assist the IO muscles in the adduction/abduction movements, aid in the extension of the IP joints when the EDC tendon, IO and LU muscles contract and, most importantly, they coordinate the passive flexion/extension of the DIP joint with the PIP joint [10].

As it can be noticed, the human finger possesses a highly complex and redundant tendon network via the extensor mechanism. In our work, no attempt was made to exactly reproduce the complex arrangement of the natural finger's tendon network. Instead, we have identified the tendons and their attachments on the bones that are crucial in mimicking the finger functionally. The resulting tendon arrangement of our biomimetic finger is presented in Section V.

IV. SMA Artificial Muscle Wire

Biomimetic design approach in robotics has prompted researchers to pursue the development of new actuation materials that exhibit life-like behavior. Two such materials are SMAs and EAPs. While EAPs have high strain ratios as well as operational similarity to biological muscles, they are still at an early stage of research and are not robust enough (low bandwidth and actuation force) for robotic or prosthetic hand applications. More information regarding EAPs and their potential as artificial muscles can be found in [11].

SMAs refer to a group of metallic materials that exhibit the ability to return to their original shapes when heated up (e.g., by an electrical current) to certain phase transition temperatures. This thermo-mechanical transformation is referred to as Shape Memory Effect (SME), which is caused by a temperature and stress dependent shift in the material's crystalline structure between two phases: austenite and martensite. As the SMA wire heats and reaches the high-temperature austenite phase, the wire contracts and hardens. When the wire cools, its crystalline structure changes to the low-temperature martensite phase, at which point the wire relaxes and can be easily lengthened with an external force. (See [14] for more details on SMA properties.)

The direct-drivable SMA wires behave like the biological muscle: the wire contracts upon electrical activation, yielding forces that can be used for actuation. Other advantages of SMA wires include: light weight, compactness, high force to mass ratio and noiseless operation, which are all important attributes to prosthetic hand application. Their limitations include: dependence of the bandwidth on heating and cooling rates, limited life cycle, nonlinear effect such as hysteretic behavior, as well as the large length of wire required to create significant motion.

In this paper, the nickel-titanium (Ni-Ti or nitinol) SMA is chosen as the artificial muscle. Nitinol has been proven to be the most appropriate SMA for engineering applications. It has greater ductility, higher recovery to deformation ratio, excellent resistance to corrosion, stable transformation temperatures, high biocompatibility and ability for shape recovery by simple electric heating [12].

V. Design of the Biomimetic Finger – Index finger

A. Finger Dimensions

Values for the index finger's average cross-sectional breadth and depth at the approximate centre of each joint, for extended finger joints, are presented in [13]. Furthermore, the ratios of the joint center locations with respect to the phalanx lengths are presented in [14]. However, these dimensional data do not refer to the absolute phalanx lengths themselves. As such, a survey of the index finger size of 16 individuals was performed. Phalangeal lengths were measured (for the extended finger) between the approximate centers of the MCP, PIP and DIP joints for the proximal and middle phalanges' lengths and between the DIP joint and fingertip for the distal phalanx length. Measurements of the cross-sectional breadths and depths of the finger were also made at the approximate center of each joint. This survey yielded dimensional values that were comparable to those listed in [13] and [14]. However, note that in prosthetic design, owing to large variations in hand dimensions from one person to another, prostheses are usually customized to dimensionally fit a person's hand.

TABLE 1
Finger Dimensions

Length (mm)			**Breadth (mm)**			**Depth (mm)**		
Proximal	Middle	Distal	MCP	PIP	DIP	MCP	PIP	DIP
34.00	22.50	18.00	15.00	14.25	12.50	15.00	13.13	10.38

Since our finger design further aimed a modeling a child's finger, a scale factor of 0.75 was applied with our measurements. The resulting dimensional values used in this work are summarized in Table 1.

B. Kinematic Architecture

Our biomimetic finger consists of three links corresponding to the three phalanges of the human finger. The finger is equipped with 3 active DOFs – 2 at the MCP joint and 1 at the PIP joint - and a passive DOF at the DIP joint. Buchholz et al. [13] suggested that an anatomical estimate of the joint center location can be defined at the head of the bone proximal to the given joint. Furthermore, these joint center locations remain fixed along the entire range of motion of the phalanges [14].

Transposing these features to our biomimetic model, fixed axes of rotations were implemented at the head of the phalanges, for the DIP and PIP joints, by modeling them as revolute hinge joints (see Fig. 6). In these joints, the rotation occurs about a fixed shaft common to the head of the proximal phalanx and the base of middle phalanx for the PIP joint and the head of the middle phalanx and the base of the distal phalanx for the DIP joint. The 2 DOF articulation of the MCP is modeled using a universal ball joint, which mimics the biaxial nature of the human finger's MCP joint. The range of motions at the modeled joints reflects the joint range of the human index finger: flexion/extension of 90^o and adduction/abduction of 20^o at the MCP joint, flexion/extension of 100^o at the PIP joint and 80^o at the DIP joint. The MCP joint motion is restrained in two orthogonal planes by securing the proximal phalanx with tendon cables. The MCP adduction/abduction joint range is limited through artificial muscle actuator control whereas the maximum flexion limit of 90^o at this joint is implemented via a mechanical stop. Similarly, the flexion limits at the PIP and DIP joints are also achieved by mechanical stops, incorporated within the structure of the links. Fig. 5 shows the proposed finger kinematic architecture.

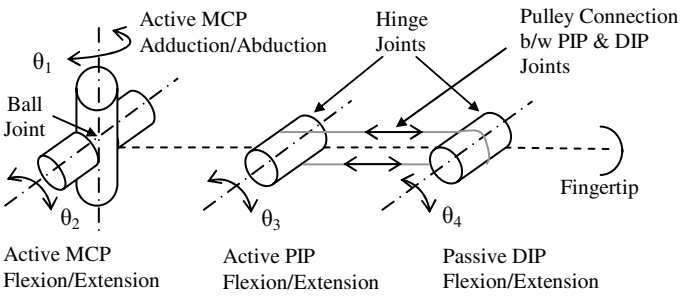

Fig. 5. Proposed finger kinematic architecture

C. Actuation Mechanism

As shown in Fig. 6, a hybrid actuation mechanism is proposed where the MCP and PIP joints are tendon-driven and the DIP joint is passively connected to the PIP joint by a pulley mechanism. The commonly used 2N tendon arrangement is adopted for the finger actuation, where N is the number of active DOFs in the finger, i.e., N = 3 (2 at the MCP joint plus 1 at the PIP joint). The action of the lateral bands (see Fig. 4), which passively connect the PIP and DIP joints, is mimicked by incorporating a pulley mechanism in the finger design. This has the added advantage of reducing the number of actuators required and, consequently, simplifying the control of the two joints. Pulley diameters are selected so that both PIP and DIP joints reach their maximum flexion/extension limits simultaneously.

The tendons are inextensible wires connected to the finger structure at the locations similar to those of the human index finger. Functionally, these artificial tendons replicate the action of the extrinsic tendons (FDS, FDP and EDC) and intrinsic muscles (IO and LU). As illustrated in Fig. 6, these artificial tendons are: two extensor tendons for extension of the MCP and PIP joints, two flexor tendons for flexion of the same joints, and two adduction/abduction tendons for the MCP joint. In addition, there is the passive flexion/extension tendon connecting the pulleys located on the shafts of the PIP and DIP joints. The hybrid actuation mechanism eliminates the need for complex transmission systems within the restricted space of the finger structure.

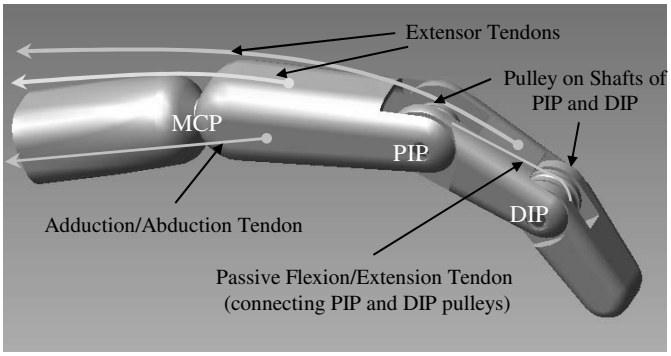

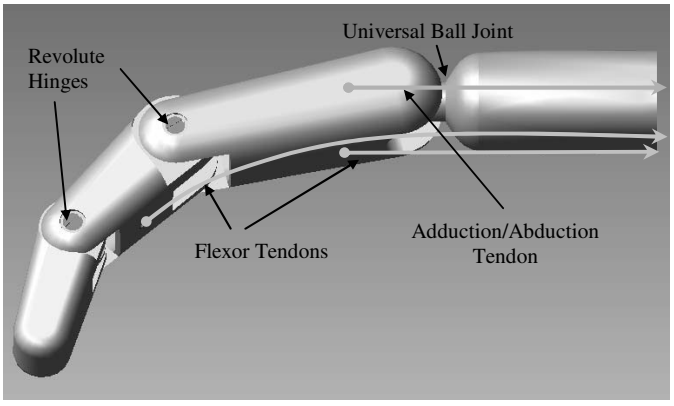

Fig. 6. CAD model of the biomimetic prosthetic finger

The tendon wires are connected to SMA artificial muscle wires placed remotely to the finger joints. Once the complete prosthetic hand is built, the SMA wires will be placed within the palm of the hand. An agonist-antagonist mechanism (see Fig. 7) is employed using two opposing SMA wires, in which the bias force is provided by the opposing SMA wire. In the neutral position, Wire 1 is in its stretched state while Wire 2 is in its

contracted state. As illustrated Fig. 7, a clockwise joint rotation (i.e., flexion) is performed by the activation (or contraction) of Wire 1 that forcefully stretches Wire 2. When Wire 1 cools and relaxes, Wire 2 can be activated to return the joint to its original position. Note that the wires should not be activated at the same time. The bandwidth of these wires mainly depends on the cooling, which is related to the thickness of the wires (thin wires cool faster than thicker ones) and the surrounding cooling condition (e.g., ambient temperature). Hence, in order to increase strength but also retain a fast bandwidth, several thin wires can be placed in parallel.

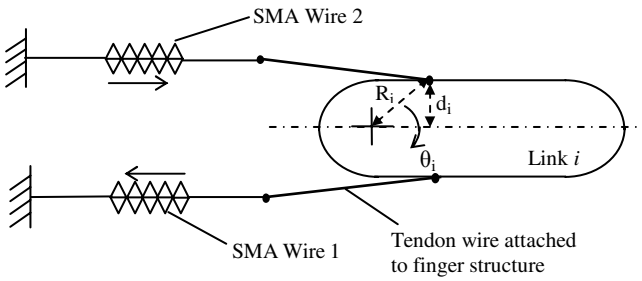

Fig. 7. SMA driven agonist-antagonist tendon pairs for link *i*

Chao et al. [1] presents the exact location of each natural tendon on the finger bones. These values are used as a basis for our tendon wire placements. A further consideration, however, involved defining tendon wire locations that would minimize the subsequent SMA wire force requirements. In an unopposed (i.e., without bias force) joint flexion, the flexion moment is measured at each joint by multiplying the tension in the flexor tendon and the perpendicular distance from the tendon to the axis of the joint, which is equal to the cross-sectional radius of the finger. In our design, since this cross-sectional value does not vary substantially along link lengths, the tendons can be attached anywhere along the links without significantly altering the required actuator force values. The biomimetic finger tendon locations are shown in Fig. 6.

VI. Finger Kinematics

A kinematic analysis of the finger is carried out in order to determine the relationship between the angular position of each joint and the required SMA contraction/elongation. The finger was modeled as a robot fixed to the palm. The Modified Denavit-Hartenberg notation, which represents the kinematic structure of a robot by a series of transformation between successive links of the kinematic chain, was used.

We start by solving the forward kinematic problem where individual link transforms are concatenated to yield a single transform that fully describes the position and orientation of the fingertip with respect to the base reference frame (located in the palm and assigned at the intersection of the proximal and metacarpal bone). Evaluation of the finger joint angles, that is the inverse kinematics solution, basically involves manipulating of the set of non-linear equations produced by the forward kinematic solution (see Appendix A).

The input to the inverse kinematic problem would, in our case, be the *x*, *y* and *z* coordinates of the fingertip. However, the prosthetic finger is a 4 DOF finger that is being used for a 3 DOF positioning task. As such, a 1 DOF redundancy exists, which complicates the inverse kinematics problem since the Cartesian coordinates of the fingertip are not sufficient to solve the set of non-linear equations presented in Appendix A. Various methods are available in literature to deal with redundant systems. However, a simple and straightforward approach is presented in [15], which is adopted in our work. The redundancy issue is resolved by specifying a fingertip orientation angle with respect to the base reference frame, in addition to the fingertip Cartesian position information. This orientation angle, α, is measured between the *x*-axis of the base reference frame and the *x*-axis of the fingertip frame as shown in Fig. 8. With this additional parameter, the finger joint values can be fully defined. The joint equations of the inverse kinematic solution are presented in Appendix B.

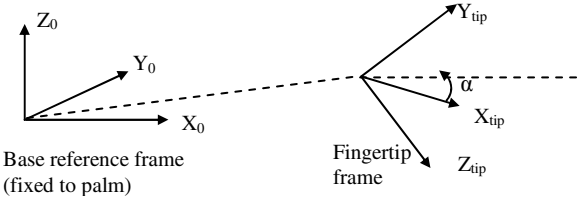

Fig. 8. Fingertip orientation angle α

Let the contracting SMA wire that causes clockwise rotation (flexion) be denoted as Wire 1 and the opposing SMA wire be referred as Wire 2, as shown in Fig. 7. Then, at actuation, the lengths l_{1i} and l_{2i} of Wires 1 and 2 are related to the joint angle θ_i by the following equations:

$$l_{2i} = l_{2o} + R_i(\theta_{0i} - \theta_i) \quad (1)$$

$$l_{1i} = l_{1o} - R_i(\theta_{0i} - \theta_i) \quad (2)$$

where: l_{1o} = initial SMA Wire 1 length
l_{2o} = initial SMA Wire 2 length
θ_{0i} = initial joint angle of joint *i*
R_i = radius of rotation as illustrated in Fig. 7.

TABLE 2
SMA Wire Contraction/Elongation

Joint Motion	Max. Joint Range	Max. SMA Wire Contraction/Elongation
MCP Adduction/Abduction	20 °	3.81 mm
MCP Extension/Flexion	90 °	16.72 mm
PIP Extension/Flexion	100 °	25.29 mm

It should be noted that, in the above, the clockwise rotation is defined as a negative rotation. Table 2 shows the required SMA elongation/contraction when the finger joints move through their maximum ranges of motion.

VII. Static Torque Analysis

One major consideration in designing prosthetic hands is the

ability to hold an object in a stable grasp. In this section, the joint torques that are sufficient to sustain such a grasp are evaluated for different finger configurations.

For this preliminary analysis, some assumptions are made. Firstly, only externally applied forces will be considered, i.e., the forces acting on the finger when grasping or pushing an object. This means that any internal forces owing to the compliance of the finger structure and joint friction are assumed negligible. Secondly, a point contact model with friction is used for the external forces, i.e., each contact point on the finger, by an object, exerts a pure force, normal and tangential to the finger surface. No moments are exerted. Thirdly, the joint torques equations are evaluated for fingertip forces only.

It can be shown that the transpose of the finger Jacobian maps the Cartesian forces acting on the fingertip into equivalent joint torques according to the following equation [16]:

$$\tau = J^T F \tag{3}$$

where F is the Cartesian force-moment vector acting at the fingertip, τ is the joint torque vector and J is the finger Jacobian. This equation is used to evaluate the joint torques necessary for static equilibrium of the finger during grasping. The static torque equations derived from (3) are presented in Appendix C.

Chao et al. [1] defines the joint orientation angles for the human index finger for various functions of the hand, as well as the externally applied forces required to simulate these functions. The magnitude, orientation and point of application of the forces along the finger are described for force magnitudes normalized to one. However, since our torque equations cater for fingertip forces only, force-moment transforms are used to express these manipulation and grasping forces as forces acting on the fingertip. The transformed manipulation and grasping forces are summed up and expressed as a resultant force acting on the fingertip (proposed by Venkataraman and Iberall [2]). The resultant fingertip force-moment vector obtained for each finger configuration is used in (3) and the corresponding index finger's static joint torque values are evaluated. Table 3 summarizes joint torques for different finger configurations and for unit normalized forces acting on the finger. τ_1 and τ_2 refer to the torques at the MCP joint owing to adduction/abduction and extension/flexion, respectively; and τ_3 and τ_4 are the PIP and DIP joint torques, respectively.

VIII. Actuator Specifications

Table 3 presents the joint torques for unit forces acting on the finger. To determine the actual joint torques, these values need to be multiplied by a factor equivalent to magnitude of the force at the fingertip. Other studies indicate that a maximum force of 5.7 N occurs at the index fingertip, for the average adult, during static grasping [17]. Applying a scale factor of 0.5 to represent child's hand, the index fingertip force of 2.85 N is used to calculate the actual torques at the joints of our biomimetic finger.

In static analysis, the torque at joint i is given by the following equation:

$$\tau_i = F_{1i} d_i - F_{2i} d_i \tag{5}$$

where: F_1 = actuation force of Wire 1

F_2 = opposing force of Wire 2

d_i = finger cross-sectional radius at tendon location (as illustrated in Fig. 7.)

In terms of the stress in the wires and assuming identical wires are used, equation (5) can be written as:

$$\tau_i = \sigma_{1i} A_i d_i - \sigma_{2i} A_i d_i \tag{6}$$

where: σ_1 = actuation stress in Wire 1

σ_2 = opposing stress in Wire 2

A_i = cross-sectional area of SMA wires located at joint i

TABLE 3
Joint Torques Values for Unit Force Generated at Fingertip (index finger)

Finger Configuration	τ_1 (Nmm)	τ_2 (Nmm)	τ_3 (Nmm)	τ_4 (Nmm)	Joint Angles (°)			Point of Application
					DIP	PIP	MCP	
Pinch Grip	0	50.58	21.14	0	25	50	3	Distal
Lateral Pinch	42.06	0	0	0	20	35	25	Middle
Palm Pinch	0	49.77	15.91	0	0	50	3	Distal
Grasp	0	39.51	1.72	40.03	23	48	0	Distal, Middle, Proximal
Adduction	56.50	0	0	0	0	0	0	Middle
Abduction	56.50	0	0	0	0	0	0	Middle
Flexion	0	56.50	22.50	0	0	0	45	Distal
Extension	0	0	34.00	56.50	0	0	0	Proximal
Cylindrical Grip	0	10.51	0	22.49	55	72	18	Middle

The wire cross-sectional area can, therefore, be expressed in terms of the wire stress values:

$$A_i = \frac{\tau_i}{d_i(\sigma_1 - \sigma_2)} \quad (7)$$

SMA actuator design calculations require the maximum tensile stress at high temperature and strain of the SMA wire at low temperature to be specified [18]. To ensure that the maximum SMA wire fatigue life is obtained, a typical high temperature tensile stress of 170 MPa is used for Ni-Ti alloys [18]. Furthermore, the recommended bias force that should be applied to extend a cooled SMA wire is 35 MPa [19]. Next, we consider the maximum torques that can occur at each joint. From Table 3, maximum torque values are observed at the MCP joint during adduction/abduction and flexion motions and, in the case of PIP and DIP joints, at extensions. It should be noted that since, rotation at the PIP joint induces rotation of the DIP joint, the PIP joint torque value must account for the DIP joint torque also. Assuming no power loss in the transmission, the net power input at the PIP joint can be considered as the summation of the power required to drive the PIP and DIP joints. Hence, net torque requirement at the PIP joint is given by:

$$\tau_{PIP} = \tau_3 + r\tau_4 \quad (8)$$

where r is the diameter ratio between the two pulleys on the PIP and DIP joints.

Using the above defined stress constraints (170 MPa for Wire 1 and 35 MPa for Wire 2) and the maximum torque values in Table 3, the minimum wire diameter necessary to ensure adduction/abduction of the MCP joint and flexion of the MCP, PIP and DIP joints can be calculated, based on the maximum fingertip force of 2.85 N. These values are presented in Table 4. Note that it is assumed that identical opposing SMA wires are used. Hence, the wire diameters presented in Table 4 also correspond to Wire 2. The maximum SMA actuation forces required for Wire 1 are also given. If higher bandwidths are required, the actuation force can be distributed into multiple SMA wires of smaller diameter and acting in parallel.

TABLE 4
DIAMETER, LENGTH AND ACTUATION FORCES FOR SMA WIRE 1

Joint Motion	SMA Wire Diameter (μm)	SMA Wire Length (mm)	Max. Actuation Force (N)
Adduction/ Abduction	582	95.3	35.2
MCP Flexion	582	418	35.2
PIP Flexion	689	632.3	49.3

The chosen maximum low temperature strain for this work is 4%. This strain value corresponds to the SMA wire elongation/contraction presented in Table 2. From the above, the SMA wire lengths can be calculated:

$$l = \frac{\Delta l}{\varepsilon} \quad (9)$$

where: l = SMA wire length
Δl = SMA wire contraction/elongation
ε = maximum allowable strain

The wire lengths, for a maximum strain of 4%, are also presented in Table 4.

IX. CONCLUSION / FUTURE WORK

This paper presents a biomimetic prosthetic finger designed to mimic the kinematic architecture of the natural index finger. A 4 DOF finger, actuated by SMA artificial muscles, is proposed. A kinematic study of the finger has defined the relationship between the SMA wires' elongation/contraction and the finger joint angles. Hence, a particular finger configuration can be achieved by adequately controlling agonist-antagonist SMA wire lengths at each joint. This preliminary study has also identified the required finger joint torques for stable finger grasping configurations. The SMA wires' diameters, lengths as well as the maximum actuation forces necessary to produce adduction/abduction at the MCP and flexion at the MCP, PIP and DIP have been calculated. Future work includes the possible use of SMA wire bundles to accommodate the large strain/force bandwidth requirements for our finger design. A nonlinear modeling of SMA artificial muscle wires and synthesis of biomimetic control algorithms to study the finger's closed-loop performance will also be performed. Fig. 8 shows a prototype of the biomimetic finger fabricated using the rapid prototyping technique. This finger prototype will be used as platform for the testing of our SMA artificial muscle actuation scheme.

Fig. 9. Prototype of biomimetic finger

APPENDICES

Appendix A: Forward Kinematic Solution

$$p_x = L_3 s_{234} + c_1(L_2 c_{23} + L_1 c_2)$$
$$p_y = L_3 s_1 s_{23} + s_1(L_2 c_{23} + L_1 c_2)$$
$$p_z = L_3 c_{234} + L_3 s_{23} + L_1 s_2$$

in which L_1, L_2 and L_3 are the proximal, middle and distal link lengths, respectively; p_x, p_y and p_z are the Cartesian

coordinates of the fingertip; $\cos\theta_i = c_i$, $\sin\theta_i = s_i$, where i = 1, 2, 3 and 4 corresponding to the MCP adduction/abduction and MCP, PIP and DIP flexion/extension angles as denoted in F; and also $\cos(\theta_i + \theta_j) = c_{ij}$, $\sin(\theta_i + \theta_j) = s_{ij}$, $\cos(\theta_i + \theta_j + \theta_k) = c_{ijk}$ and $\sin(\theta_i + \theta_j + \theta_k) = s_{ijk}$, where i, j, k = 2, 3, 4, corresponding to the MCP, PIP and DIP joint extension/flexion.

Appendix B: Inverse Kinematic Solution

$$\theta_1 = a\tan 2(p_y, p_x) + n\pi \quad (n = 0, 1)$$

$$\theta_2 = a\tan 2(s_2, c_2), \quad \theta_3 = a\tan 2(s_3, c_3)$$

$$\theta_4 = a\tan 2(-(o_x c_1 + o_y s_1), o_z) - (\theta_2 + \theta_3)$$

where:
$$s_2 = \frac{(L_2 c_3 + L_1) p'_z - L_2 s_3 p'_x}{L_1^2 + L_2^2 + 2L_1 L_2 c_3}$$

$$c_2 = \frac{(L_2 c_3 + L_1) p'_x + L_2 s_3 p'_z}{L_1^2 + L_2^2 + 2L_1 L_2 c_3}$$

$$c_3 = \frac{(p'_x)^2 + (p'_z)^2 - L_2^2 - L_1^2}{2L_1 L_2}$$

$$s_3 = \pm\sqrt{(1 - c_3^2)}$$

$$p'_x = L_2 c_{23} + L_1 c_2, \quad p'_z = L_2 s_{23} + L_1 s_2$$

in which o_x, o_y and o_z are the components of the forward transformation matrix describing the fingertip position and orientation with respect to the palm of the hand.

Appendix C: Joint Torque Equations

$$\tau_1 = J_{11} f_x + J_{12} f_y + m_z$$

$$\tau_2 = J_{21} f_x + J_{22} f_y + J_{23} f_z + J_{24} m_x + J_{25} m_y$$

$$\tau_3 = J_{31} f_x + J_{32} f_y + J_{33} f_z + J_{34} m_x + J_{35} m_y$$

$$\tau_4 = J_{41} f_x + J_{42} f_y + J_{43} f_z + J_{44} m_x + J_{45} m_y$$

where:
$$J_{11} = -L_3 s_1 c_{234} + L_2 c_{23} + L_1 c_2$$

$$J_{12} = L_3 c_1 c_{234} + L_2 s_{23} + L_1 c_2$$

$$J_{21} = -L_3 c_1 s_{234} - L_2 s_{23} - L_1 s_2$$

$$J_{22} = -L_3 s_1 s_{234} - L_2 s_{23} - L_1 s_2$$

$$J_{23} = L_3 c_{234} + L_2 c_{23} + L_1 c_2$$

$$J_{24} = J_{34} = J_{44} = s_1$$

$$J_{25} = J_{35} = J_{45} = -c_1$$

$$J_{31} = -L_3 c_1 s_{234} - L_2 s_{23}$$

$$J_{32} = -L_3 s_1 s_{234} - L_2 s_{23}$$

$$J_{33} = L_3 c_{234} + L_2 c_{23}$$

$$J_{41} = -L_3 c_1 s_{234}$$

$$J_{42} = -L_3 s_1 s_{234}$$

$$J_{43} = L_3 c_{234}$$

in which f_x, f_y, f_z, m_x, m_y and m_z are the Cartesian components of the force-moment vector at the fingertip.

REFERENCES

[1] Chao, E.Y.S., An, K., Cooney, W.P. and Linscheid, R., *Biomechanics of the Hand*, Teaneck, NJ. USA: World Scientific Publishing Co. Pte. Ltd., 1989, pp. 5-75.

[2] Venkataraman, S.T. and Iderall, T., Dexterous Robot Hands, New York, NY: Springer-Verlag New York Inc., 1990, pp. 136-149.

[3] Guo, G., Gruver, W.A. and Qian, X., "A Robotic Hand Mechanism with Rotating Fingertips and Motor-Tendon Actuation", Proc. of the 1991 IEEE International Conference of Systems, man and Cybernetics, vol.2, pp. 1023-1028, Charlottesville, VA, Oct 1991.

[4] Siegel, D.M., Kriegman, D.J., Narasimhan, S., Gerpheide, G.E. and Hollerbach, J.M., "Computational Architecture for the UTAH/MIT Hand", Proc. of the 1985 IEEE International Conference on Robotics and Automation, vol. 2, pp. 918-924, Mar 1985.

[5] Carrozza, M.C., Massa, B., Micera, S., Lazzarini, R., Zecca, M. and Dario, P., "The Development of a Novel Prosthetic Hand – Ongoing Research and Preliminary Results", *IEEE/ASME Transactions on Mechatronics*, vol. 7, no. 2, pp. 108-114, June 2002.

[6] Schulz, S., Pylatiuk, C. and Bretthauer, G., "A New Ultralight Anthropomorphic Hand", *Proc. of the 2001 IEEE International Conference on Robotics & Automation*, vol. 3, pp. 2437-2441, Seoul, Korea, May 2001.

[7] Landsberger, S., Shaperman, J., Setoguchi, Y., Fite, R., Lin, A., Vargas, V. and McNeal, D., "Child prosthetic hand design: no small challenge", *Proc. of the 1996 Wescon Conference*, pp. 236-240, Oct 1996.

[8] Levangie, P.K. and Norkin, C.C., *Joint Structure and Function: A comprehensive Analysis*, 3rd ed., Philadelphia, PA: F.A Davis Company, 1992, pp. 265-285.

[9] Folgheraiter, M. and Gini G., "Blackfingers: an Artificial Hand that Copies Human Hand in Structure, Size and Functions", *Proc. of the IEEE Conference on Humanoids 2000*, MIT, Cambridge, MA, Sept 2000.

[10] Wilkinson, D.D., Vande Weghe, M., Matsuoka, Y., "An Extensor Mechanism for an Anatomical Robotic Hand", *Proc. of the 2003 IEEE International Conference on Robotics and Automation*, Taipei, Taiwan, Sept 2003.

[11] Bar-Cohen, Y., *Electroactive Polymer (EAP) Actuators as Artificial Muscles – Reality, Potential and Challenges*, Bellingham, WA: SPIE-The International Society for Optical Engineering, 2001, pp. 4-37.

[12] Mavroidis, C., "Development of Advanced Actuators Using Shape Memory Alloys and Electrorheological Fluids", *Research in Nondestructive Evaluation*, vol. 14, no. 1, pp. 1-32, Mar 2002.

[13] Buchholz, B. and Armstrong, T., "Ellipsoidal representation of human hand anthropometry**",** *Human Factors*, vol. 33, no. 4, Aug 1991, pp. 429-441.

[14] Buchholz, B., Armstrong, A., and Goldstein, S.A., "Anthropometric data for describing the kinematics of the human hand", *Ergonomics*, vol. 35, no. 3, March 1992, pp. 261-273.

[15] Narasimhan, S., *Dexterous Robotic Hands: Kinematics and Control*, Technical Report, Artificial Intelligence Laboratory, MIT, 1988, pp. 19-31.

[16] Craig, J.J, Introduction to Robotics, Mechanics and Control, 2nd ed., Don Mills, Ontario: Addison-Wesley Publishing Company Inc., 1989, pp. 69-186.

[17] Kargov, A., Pylatiuk, C., Martin, J., Schulz, S. and Doderlein, L. "A comparison of the grip force distribution in the natural hands and in prosthetic hands", Disability and Rehabilitation, vol. 26, no. 12, 2004 pp. 705-711.

[18] Waram, T., *Actuator Design Using Shape Memory Alloys*, 2nd ed. Ontario, Ca: T.C. Waram Publishing, 1993.

[19] Gilberston, G., *Muscle Wires Project Book*, 3rd ed., San Rafael, CA: Mondo-tronics, 1993